COEXISTENCE OF FAST AND SLOW SLIP EVENTS IN LABORATORY SEISMIC CYCLES

Kseniya G. Morozova[1], Vadim K. Markov[1], Dmitry V. Pavlov[1], Maxim F. Popov[2], and Alexey A. Ostapchuk[3]

[1]Sadovsky Institute for Dynamics of Geospheres of Russian Academy of Sciences
[2]Bauman Moscow State Technical University
[3]Moscow Institute of Physics and Technology

November 23, 2022

Abstract

The spectrum of slip modes on gouge-filled faults spans a continuum from fast ruptures to slow slip events. The nucleation of a certain slip mode is governed by the frictional heterogeneity of fault interface and the rheological fault stiffness. Though the pattern of mechanical parameter variation and dynamic stability loss during a seismic cycle is quite clear, it is important to have a unified seismic-acoustic signature of slow or fast slip event nucleation. We present laboratory acoustic emission (AE) experiments on a slider-model with a precise control of mechanical and AE parameters. A comprehensive analysis of AE activity points to the presence of two AE subpopulations. One of them manifests as pulses with harsh onsets. The second one exhibits a gradual amplitude rise and tremor-like signal. The second AE subpopulation shows a longer failure duration and increased energy dissipation. Regularities of changing the frequency-amplitude characteristics of AE subpopulations during a laboratory seismic cycle differ. The first AE subpopulation retains parameters of frequency-amplitude distribution, but the second one exhibits a pronounced cyclic recurrence of the *b-value*. The latter decreases before slip events and recovers after them. The detected features of AE subpopulations are common for the entire spectrum of slip modes. Findings reveal a coexistence of slow and fast modes at the same fault at the micro-scale and point to the unity of underlying physical mechanisms of different slip mode nucleation.

Hosted file

`supplementary materials - morozova et al._31.07.docx` available at https://authorea.com/users/543147/articles/601458-coexistence-of-fast-and-slow-slip-events-in-laboratory-seismic-cycles

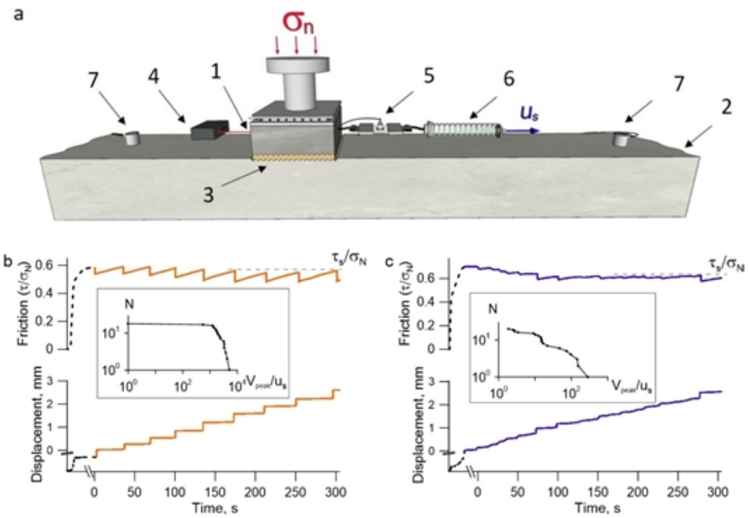
a
σn
7
4
1
5
6
7
2
us
3
b
c
τs/σN
Friction (τ/σN)
Displacement, mm
Time, s
N
Vpeak/us

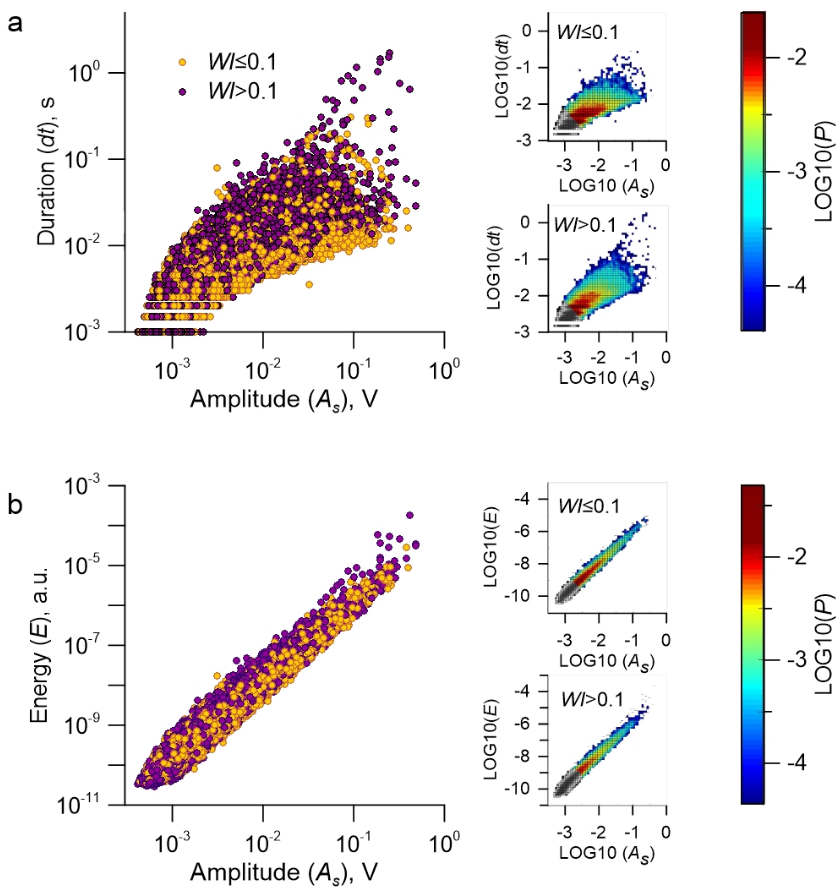
a
WI≤0.1
WI>0.1
Duration (dt), s
Amplitude (As), V
LOG10(dt)
LOG10 (As)
LOG10(P)
b
Energy (E), a.u.
LOG10(E)

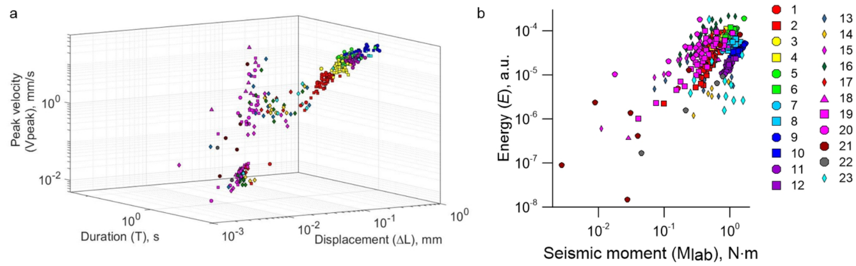
a
Peak velocity (Vpeak), mm/s
Duration (T), s
Displacement (ΔL), mm
b
Energy (E), a.u.
Seismic moment (Mlab), N·m
1
2
3
4
5
6
7
8
9
10
11
12
13
14
15
16
17
18
19
20
21
22
23

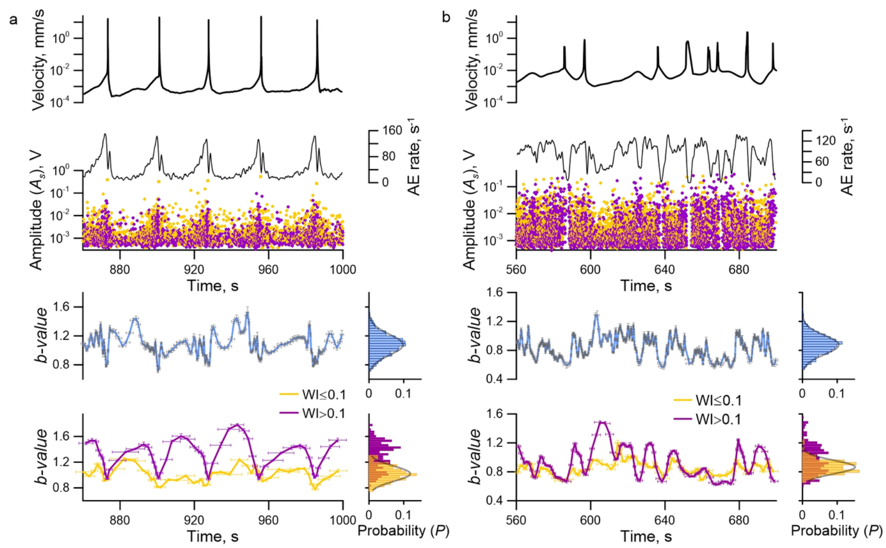
a
b
Velocity, mm/s
Amplitude (As), V
AE rate, s-1
Time, s
b-value
WI≤0.1
WI>0.1
Probability (P)

COEXISTENCE OF FAST AND SLOW SLIP EVENTS IN LABORATORY SEISMIC CYCLES

[2]K.G. Morozova, [2]V.K. Markov, [2]D.V. Pavlov, [3]M.F. Popov & [1,2,*]A.A. Ostapchuk

[1]Moscow Institute of Physics and Technology, Institutsky lane 9, Dolgoprudny, Moscow region, 141700, Russia

[2]Sadovsky Institute for Dynamics of Geospheres of Russian Academy of Sciences, Leninsky av., 38, bldg.1, Moscow, 119334, Russia

[3]Bauman Moscow State Technical University, 2d Baumanskaya str., 5, Moscow, 105005, Russia

*Corresponding authors: Alexey Ostapchuk (ostapchuk.aa@phystech.edu, ostapchuk@idg.chph.ras.ru) , Kseniya Morozova (morozova@ idg.chph.ras.ru)

The spectrum of slip modes on gouge-filled faults spans a continuum from fast ruptures to slow slip events. The nucleation of a certain slip mode is governed by the frictional heterogeneity of fault interface and the rheological fault stiffness. Though the pattern of mechanical parameter variation and dynamic stability loss during a seismic cycle is quite clear, it is important to have a unified seismic-acoustic signature of slow or fast slip event nucleation. We present laboratory acoustic emission (AE) experiments on a slider-model with a precise control of mechanical and AE parameters. A comprehensive analysis of AE activity points to the presence of two AE subpopulations. One of them manifests as pulses with harsh onsets. The second one exhibits a gradual amplitude rise and tremor-like signal. The second AE subpopulation shows a longer failure duration and increased energy dissipation. Regularities of changing the frequency-amplitude characteristics of AE subpopulations during a laboratory seismic cycle differ. The first AE subpopulation retains parameters of frequency-amplitude distribution, but the second one exhibits a pronounced cyclic recurrence of the *b-value*. The latter decreases before slip events and recovers after them. The detected features of AE subpopulations are common for the entire spectrum of slip modes. Findings reveal a coexistence of slow and fast modes at the same fault at the micro-scale and point to the unity of underlying physical mechanisms of different slip mode nucleation.

Key words: Fractures and faults, Rheology and friction of fault zones, Self-organization, Seismic cycle, Earthquake dynamics.

1. Introduction

The blocky hierarchical structure of the Earth's crust determines its movability and localization of deformations in interblock zones. Faults and large fractures control regularities of accumulation and relaxation of the energy of elastic deformation in a blocky massif (Scholz, 2002; Kocharyan, 2016). The dynamics of relaxation processes that are accompanied by slips along faults is determined by the ratio of the rheological stiffness of the fault to the one of the enclosing massif (Leeman et al., 2016; Kocharyan et al., 2017). Slip modes observed in nature span a continuum, given the heterogeneity and complexity of natural systems (Peng, Gomberg, 2010). Different faults may exhibit just fast slip modes (ordinary earthquakes), or just slow slip modes (low-frequency earthquakes, slow slip events), or even both fast and slow modes together (Villegas-Lanza et al., 2015; Veedu, Barbot, 2016; Ostapchuk et al., 2019a).

The frictional instability is the most probable mechanism of the entire continuum of fault slip modes (Schoolz, 2002; Nielsen, 2017). During fault evolution, slip events are triggered when shear stresses reach the ultimate strength at a local fault segment. In the vicinity of the ultimate strength the source stays in a metastable state, so that even a slight fluctuation of stress may lead to a loss of dynamic stability. The transition of a fault to a metastable state is accompanied by a decrease of the shear stiffness of source zone (Johnson, Jia, 2005; Kocharyan, Ostapchuk, 2011). At present we cannot measure neither stresses, nor static stiffness 'in situ'. Only indirect manifestations of fault behavior and earthquake nucleation can be detected (Frank et al., 2016; Scuderi et al., 2016; Kocharyan et al., 2018).

The laboratory experiment is a reliable tool to verify new hypotheses and assumptions. Regularities of fault evolution have also been widely modeled in laboratory (Marone, 1998; Rosenau et al., 2017). AE experiments reproduce qualitatively the main statistical laws that describe natural seismicity (Gutenberg-Richter law, Omori law, inverse Omori law) (Lei, 2003;

Johnson et al., 2013; Ostapchuk et al., 2019b; Lherminier et al., 2019). There are other qualitative similarities to natural seismicity – variations of wave propagation velocity, seismic quiescence, variations of scaling properties of seismicity and others. (Johnson et al., 2013, Ostapchuk et al., 2016; Scuderi et al., 2016). Similarity of recurrent fast and slow earthquakes has been demonstrated in laboratory experiments (Hulbert et al., 2019). Despite a noticeable progress, no reliable short-term precursors of slip events have been found so far (Cicerone et al., 2009; Rundle et al., 2011).

The existing models of seismic activity, describing a certain fault or a source zone, suggest that earthquake nucleation area is an integrated dynamic system which has a specific property of self-organizing criticality (Turcotte, 1999; De Arcangelis et al., 2016). At the initial stage damage accumulates at the micro-scale. Further evolution of the system lifts the destruction processes to higher hierarchical levels, thus, as the stresses approach the critical level, structural changes spread wider all over the system. The loss of dynamic stability manifests at the macro-scale in the form of a slip event. The more accurate the methods of detecting small earthquakes are, the more distinct are the patterns of large earthquake nucleation (Trugman, Ross, 2019).

This work is devoted to investigation of a complex acoustic pattern of simulated gouge-filled fault evolution. A large number of AE pulses (AEs) can be detected during a laboratory seismic cycle. Signals of one type resemble classical impulsive earthquakes, while the others are more tectonic tremor-like. We have shown the difference in their scaling relations. Detecting the AE fine structure and analyzing scaling characteristics have allowed to reveal specific signs of nucleating both fast and slow slip events. These results provide a new insight into the seismic event nucleation and predictability of fast and slow slip instability.

2. Experimental methods

Laboratory experiments were performed on a slider-model. A scheme of the set-up is shown in Fig. 1. The model fault – a confined granular layer between two blocks – was subjected to external normal and shear stresses. The moveable granite block (1) 8×8×3 cm^3 in size was put in the middle of the granite base rod 2.5 m long and 10×10 cm^2 in cross section. The contact surfaces of the block and the base rod were made artificially rough by introducing grooves 0.8-1.0 mm deep. The contact gap between the block and the base was filled with a granular material (3). Mixtures of different granular materials were used as fillers. All fillers are listed in the Supplementary Material. Their structural properties determined realization of a certain slip mode (Mair et al., 2002; Anthony, Marone, 2005; Kocharyan et al., 2014).

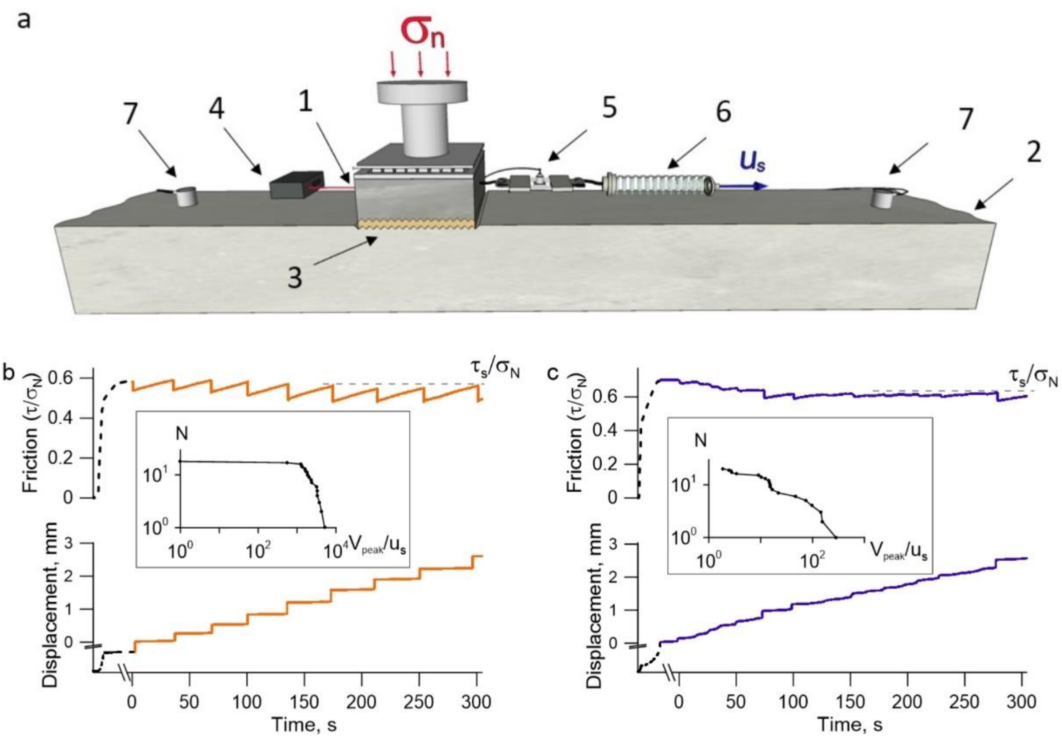

Figure 1. The slider-model performance test.

A scheme of the experimental set-up (a). Mechanical (friction and displacement) and acoustic (in the frequency band of 20-80kHz) parameters were controled during the experiments.

(1) - moveable block; (2) – base rod; (3) - gouge layer; (4) - laser sensor of displacement; (5) - force sensor; (6) – spring element; (7) - AE sensors.

Characteristic variations of friction and displacement in time for a regular stick-slip (Exp.5) (b) and a stochastic sliding regime (Exp.13) (c). The point (0,0) corresponds to the moment when the ultimate strength of model fault is reached. We study the ‘mature’ stage when the friction reaches the residual shear strength. Insets (b, c) show the statistics of the realized slip events.

The moveable block slid along the interface under the applied normal and shear forces. The normal force was F_N = 500 N in all the experiments. It was applied by a set of weights. The shear force was applied to the block through an elastic element (6) with the stiffness of K = 55 kN/m. Its free end was pulled at a constant velocity of u_s =8 μm/s. The shear force was controlled with the sensor CFT/5kN (HBM, Germany) (5) with the accuracy of 1 N. The displacement of the block relative to the base was measured with the laser sensor ILD2220-10 (Micro-Epsilon, Germany) (4) in the frequency band of 0-5kHz, with the accuracy of 0.1μm.

Typical loading curves are presented in Fig. 1b,c. The fault evolution undergoes several stages (Gerasimova et al., 1995; Scuderi et al., 2017). At the initial stage the model fault reaches the ultimate shear strength. Further accumulation of shear deformation leads to the regularization of slip behavior and the contact reaches the residual shear strength (τ_s) – the 'mature' stage. We consider the 'mature' stage for a detailed analysis. Regularities of a sliding regime are defined by structural, physical and mechanical properties of the filler. Parameters of realized sliding regimes and fillers are presented in Supplementary Table S1. Using, for example, the filler composed of moistened quartz sand with a narrow size distribution of grains, allowed to realize a regular stick-slip – quasi-periodically repeated fast slip events accompanied by drops of shear stress (Fig. 1b). On the other hand, using the quartz sand with a wide size distribution of grains resulted in a stochastic sliding regime, when slip events were occasional, and their statistics obeyed a power law (Fig. 1c).

In the course of an experiment the fault evolution was accompanied by the AE. We used a set of AE sensors VS30-V (Vallen System, Germany) to record these high-frequency vibrations. The sensors were mounted on the rod at the distances of 0.6 and 0.7m at opposite sides of the moveable block,. The sample rate f_s was 2 MHz. The operational frequency band was 20–80 kHz, so we consider acoustic manifestations of the fault sliding regimes in the "far-field zone". The background noise level A_0 was 50 dB.

We used the energetic criterion for detecting the AEs – the energy flow should exceed a certain threshold for the 'event' to be detected, according to the following relation:

$$\Pi(t) = \frac{1}{\Delta t} \sum_{t}^{t+\Delta t} \frac{A(t_i)^2}{f_s} \geq 1.5 A_{\min}^2 \qquad (1)$$

A(t) is the recorded signal filtered in the frequency band of 20-80 kHz, $A_{\min}^2$ is the variance of the signal. The factor of 1.5 was established in a preliminary analysis so that the AE catalogue would be as representative as possible. The energy flow was determined in the window Δt=0.5ms long at the steps of $\Delta t/2$. $A_{\min}^2$ was determined in 1 second intervals of AE signals before the shear load started, according to the following relation:

$$A_{\min}^2 = \frac{1}{f_s - 1} \sum_{t_i > 0}^{t_i \leq 1} \left| A(t_i) - \frac{1}{f_s} \sum_{t_i > 0}^{t_i \leq 1} A(t_i) \right|^2 \qquad (2)$$

AEs of different shapes and amplitudes were emitted in sliding. Depending on the realized sliding regime the rate of AEs varied from single "clicks" at intervals of several seconds to regularly repeating AEs at intervals of 1-2 ms. Among all the recorded AEs it was necessary to distinguish those emitted during slip events and at the stage of slip event preparation (Fig. 2).

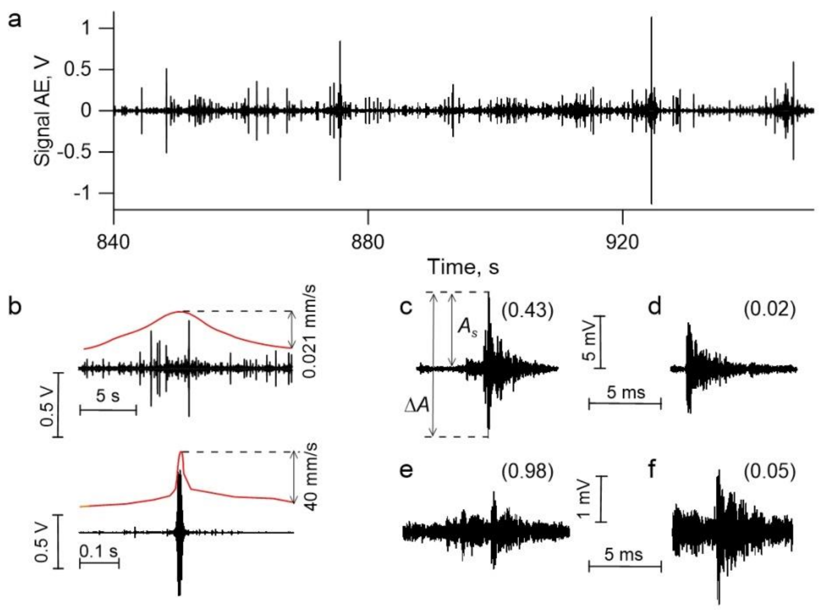

Figure 2. AE data.

The AE signal recorded during a stochastic sliding regime (Exp.13) (a). ‘Coseismic’ AEs corresponding to slip events (b) and ‘interseismic’ AEs corresponding to slip event preparation (c-f). In Fig. 2b the solid line corresponds to the time variation of block velocity. In Fig.2c-f the *WI*-value is indicated in parentheses.

The following parameters were retrieved from the detected pulses: duration (*dt*), amplitude (A_s), peak-to-peak amplitude (ΔA) and energy (*E*), which was estimated as follows:

$$E = \Delta t \sum_{t_s}^{t_e} A^2(t_i), \qquad (3)$$

It seems likely that the waveform of the pulse points to the mechanism and intensity of the evolution process inside the fault (Shiotani et al., 2001; Zigone et al., 2011; Ostapchuk et al., 2016). We have introduced a novel parameter – waveform index *WI*. *WI*-value was calculated through the formula:

$$WI = \frac{(t_{\max} - t_{\mathrm{s}})}{(t_{\mathrm{e}} - t_{\max})}, \qquad (4)$$

where t_s and t_e are the moments of beginning and termination of the pulse, t_{max} is the moment when maximum peak-to-peak amplitude is reached. Introducing the novel ‘WI-value’ parameter implies two important aspects, provided that detected are AE waves that directly reflect a source-time function (Shiotani et al., 2001; Besedina et al., 2020). First is that the gradient of the ascending part of the waveform becomes smaller as fracture propagates. Second, low-frequency components of wave-forms should be dominant with progressing fracture. It is worth mentioning that more than 95% of all the AEs registered in our experiments had *WI*-values within the range of 0 to 1. The events with the values of WI >> 1 were treated as double- or multi-pulses. They were not considered in our analysis.

3. Results

3.1. Continuum of slip events

Using mixtures of different materials, we managed to reproduce in laboratory the entire spectrum of slip modes. The fastest slip events had peak velocities up to 48 mm/s (600u_s) and the relative value of shear stress drop down to 0.1. Single high-amplitude AEs with durations corresponding to the ones of slip events were emitted in fast modes (Fig. 2b). Slow slip events had peak velocities of 2-5 u_s and durations (T) up to 5-10 s, while relative changes of shear stresses were less than 10^{-2}. The slowest slip events were accompanied by emission of a cascade of single pulses that resembled the low frequency earthquake bursts during slow slips (Fig. 2b) (Frank et al, 2016). Parameters of the realized slip events varied in wide ranges (Fig. 3). As far as the mechanical parameters are considered, one can see that all the slip events form a connected set in space (V_{peak}, T, ΔL). This point to a continuum of slip modes of fault behavior. Slip events, whose emitted energies differed by more than 1 order of magnitude, were realized in one and the same stochastic sliding regime. As far as all the experiments are considered, the difference is up to 2 orders of magnitude for events with equal "seismic moments" (Supplementary Section S1).

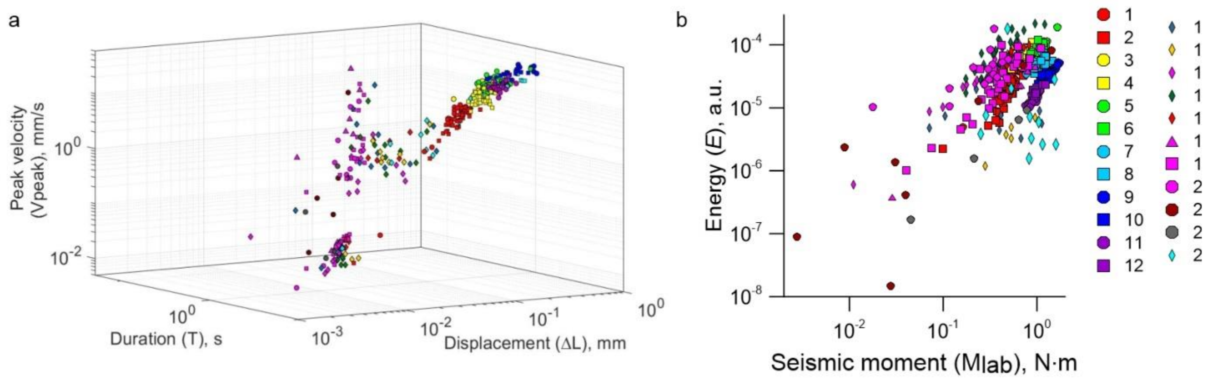

Figure 3. Variations of slip event parameters.

All slip event parameters form a connected set in the space (cumulative slip (ΔL), peak velocity (V_{peak}), slip duration (T)) (a). Comparison of laboratory 'seismic' moment and energy of 'coseismic' AE (b). The laboratory seismic moment is $M_{lab} = K \cdot \Delta L \cdot s$ (where K and s are spring stiffness and block length, respectively). The symbols correspond to different experiments listed in the Supplementary Table S1.

Though the similarity criteria are not true here, the experiments testify that the entire spectrum of sliding regimes results from the frictional instability of the model fault, just at the expense of friction. Though we do not exclude other mechanisms that may lead to formation of different slip modes, such as variations of fluid pore pressure, dehydration reactions, brittle-ductile transition and others (Reber et al., 2015; Cruz-Atienza et al., 2018; Burgmann, 2018).

3.2. Two subpopulations of AE

The change of stress-strain state of the model fault results in various structural changes and is accompanied by a great number of AEs. In general, the amplitude-frequency distribution of AEs is a superposition of a power distribution in the low-amplitude range and a peak-like distribution in the high-amplitude range (Fig. 4a).

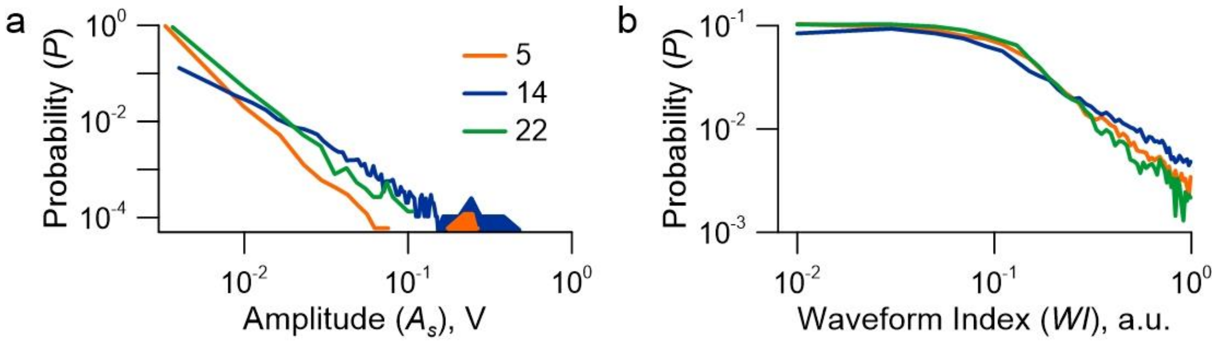

Figure 4. AEs statistics.

AEs statistics demonstrates an essential difference between amplitude-frequency (a) and waveform-frequency (b) distributions. The ‘coseismic’ AEs corresponding to slip events form the separate high-amplitude peak, which is marked by the filled area. The waveform index plot allows to detect the characteristic (cut-off) value (*WI*=0.1). Color lines are cross-referenced to numbers listed in Supplementary Table S1.

In the range of low A_s values the AEs distribution is approximated with high accuracy by the power dependence:

$$lg(N) = a - blg\left(\frac{A_S}{A_0}\right) \quad (5)$$

where N is the number of events with amplitudes not less than A_s. The value $\lg(A_s/A_0)$ corresponds to AE magnitude (Lei, 2003), a and b are two positive constants. The a-value is a measure of AE activity, which depends on the time window of observations. The slope of recurrence plot (b-value) is a scaling parameter, which characterizes the process of self-organization of the medium

(Turcotte, 1999). The power law behavior is also typical for the AE distributions over energy (*E*) and duration (*dt*).

The distribution of AEs over the *WI* parameter shows a duality, which points to the presence of two AE modes (Fig. 4b). This can be written as follows:

$$N = \begin{cases} a_{WI}, WI \leq 0.1 \\ c_{WI} \cdot WI^{-w}, WI > 0.1 \end{cases}, \tag{6}$$

where N is the number of events whose waveform parameters are not less than WI, a_{WI} and c_{WI} are positive constants, which are determined by the intensity of AE. There is also the cut-off value of WI=0.1. And it is very important. Persistence of the cut-off value in all the performed experiments, probably, points to spatial peculiarities of the internal self-organization of the medium. The index *w-value* characterizes the non-uniformity of AE ensemble over the *WI* parameter, while its alteration probably points to the predominant mechanism of AE generation. It should be noted that there is an analogous distribution for mining seismicity with the cut-off value of WI=0.23 (Besedina et al., 2020). Pulses with different *WI*-values correspond to, for example, different velocities of rupture propagation.

The essential difference of the AE distributions over amplitude and over waveform points to the necessity to consider the *WI* parameter as an independent characteristics of the process of fault evolution. The presence of a characteristic point in the waveform-frequency distribution motivates to conduct a clustering of the ensemble of detected AEs over the *WI*-value. Mode I includes AEs with $WI \leq 0.1$. They manifest as wave trains with harsh onsets. Mode II includes AEs with $WI > 0.1$. They exhibit a gradual amplitude rise.

In order to better understand the physical mechanism of internal processes of self-organization, let us consider the scaling relationships for the mode I and mode II of AE. The scaling relationships provide important insights into and constraints on the dynamics of internal processes. Fig. 5 shows log-log trends between different AE parameters. Such a presentation gives an opportunity to compare them to scaling laws for ordinary and slow earthquakes (Peng, Gomberg, 2010; Nishitsuji, Mori, 2014).

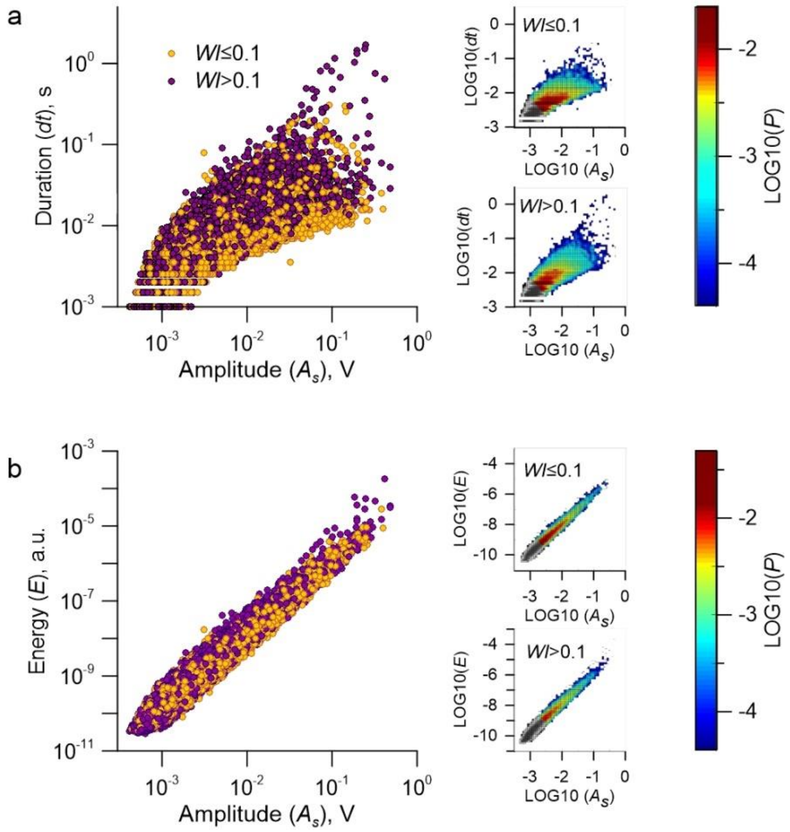

Figure 5. Scaling of two AE subpopulations in Exp.13.

(a) Duration versus amplitude of AE (mode I – yellow, mode II – purple). The complete set of AEs is limited by two solid lines given by relations (7). Right plots show the two-dimensional distribution of the AE mode I (upper) and the AE mode II (lower).

(b) AE energy versus amplitude. The energy varies by more than an order of magnitude for AEs with one and the same amplitude. Right plots show the two-dimensional distribution of the AE mode I (upper) and the AE mode II (lower).

The event duration scaling is viewed as a key to unraveling the rupture mechanism in nature and lab. All the recorded AEs form a connected set, which is limited by two boundaries:

$$\begin{aligned} dt_{upper} &\sim A_s^{1.2\pm0.2} \\ dt_{bottom} &\sim A_s^{0.5\pm0.1} \end{aligned}, \tag{7}$$

In nature this corresponds to the scaling between the seismic moment and the duration ranging from $T \sim M_0^{0.8\pm0.1}$ to $T \sim M_0^{0.3\pm0.1}$ (see Supplementary Section S2). At the same time one can see that AE mode I localizes closer to the lower boundary, than AE mode II. It means that for AEs of equal amplitudes to be realized, mode II should have a longer failure duration than mode I.

An important parameter that characterizes seismic events is the radiated energy. It varies in a wide range for slow and fast earthquake. Our analysis shows that there is an increase of the value of radiated energy with AE amplitude, and the variation of radiated energy reaches one order of magnitude for equal-amplitude AEs. Moreover, we revealed that a statistically significant difference of scaling indexes for different AE modes is observed (Supplementary Figure S1). For the AE mode I a slower growth of radiated energy with scale is observed, than for the AE mode II. Hence, the mode II exhibits an increased energy dissipation at the micro-scale.

The obtained scaling relationships clearly point to the complexity of evolution processes taking place at the micro-scale. A wide spectrum of AEs is radiated during deformation. They can be qualitatively divided into AEs that correspond to fast events (mode I) and the ones corresponding to slow events (mode II). To understand the fundamental differences between the detected AE modes, it will be appropriate to consider the model fault as a complex two-component dynamic system. Fig. 6 shows variations of mechanical and acoustic parameters for regular and stochastic sliding regimes. In order to investigate the temporal evolution of the *b-value,* we calculated *b-values* using the method of least squares in a running window for an equal number of events (nn = 100) with a running step of nn/2 events (50% overlap).

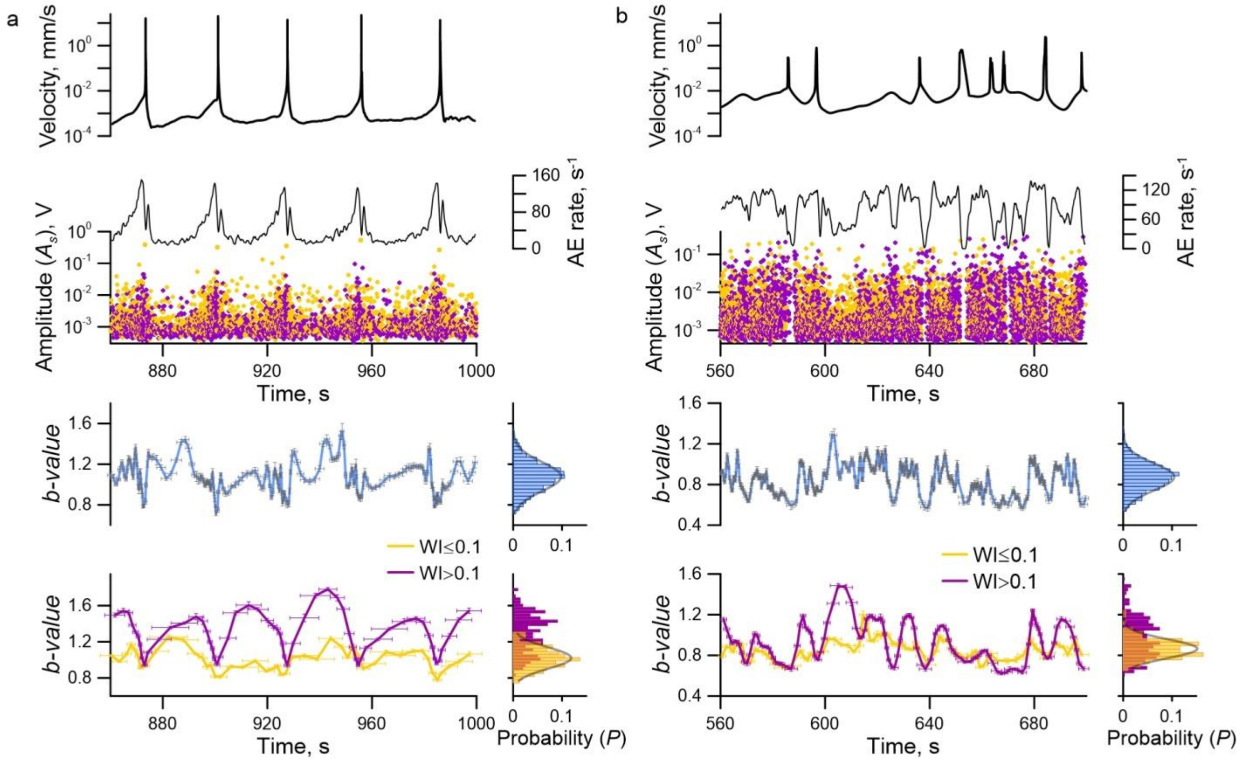

Figure 6. Evolution of model fault state.

Variations of sliding velocity and AE parameters for a regular stick-slip (Exp.3) (a) and a stochastic sliding regime (Exp.13) (b).

Unlike the stochastic regime, the regular regime shows a high correlation between the sliding velocity and the AE rate. Occasional variations of *b-value* are observed for both regular and stochastic regimes for the complete set of AEs. Histograms of *b-value* obey the normal distribution law.

Separation of AEs into two subpopulations shows an essential difference of time variations of *b-value*. Occasional alterations are observed for the AE mode I (*WI*≤0.1), while the AE mode II (*WI*>0.1) shows systematic variations.

A stable repeated pattern of variations of both mechanical and acoustic parameters is observed during a regular stick-slip. Variations of block velocity and AE rate testify three typical stages of a seismic cycle. After the dynamic failure, the post-seismic stage is observed with a decreasing velocity of block sliding and AE rate. The lowering activity is described by the law of Omori-Utsu (Lherminier et al., 2019; Ostapchuk et al., 2019b). Then approximately stable minimal values of velocity and AE rate are observed at the inter-seismic stage. As the system approaches a slip event, an accelerated block sliding is observed accompanied by an increase of AE rate. At the pre-seismic stage AE variations can be described by the inverse Omori's law (Ostapchuk et al., 2019b; Johnson et al., 2013). No clear staging of a seismic cycle is observed when analyzing variations of the *b-value* of the complete population of AE. The *b-value* distribution obeys the normal law. It should be noted that the cyclicity (but not the staging) of *b-value* alterations in a limited range of AE amplitudes has been mentioned in a few works (Reviere et al., 2018; Lei et al., 2018). Clustering AEs into two modes eliminates the ambiguity of the pattern of *b-value* variations. For a regular stick-slip the analysis of *b-value* histograms shows that the AE mode I ($WI \leq 0.1$) exhibits an almost constant *b-value* and time variations are occasional (histogram obeys the normal distribution). At the same time the AE mode II demonstrates certain periodic variations of *b-value*, and the histogram cannot be approximated by a normal distribution. If we look at the laboratory seismic cycle just after a dynamic failure at the first stage of fault recovery, we can see that a fast growth of *b-value* occurs. It means that low-amplitude AEs with gradual amplitude rise start to prevail. Then the stage of creep comes at a minimal velocity, and *b-value* remains almost constant, which for the presented case manifests as a peak in the *b-value* histogram around the value of 1.4. At the final 'pre-seismic' stage a monotonic decrease of *b-value* is observed, which means that the share of high-amplitude AEs of mode II grows.

In a stochastic regime the pattern of parameter alteration is much more complicated. It seems impossible to detect stages of the cycle through AE rate and sliding velocity. Small relative variations of AE rate are observed before slip events, while abrupt drops occur only after fast dynamic failures. There are no unambiguous variations of *b-value* over the complete population of AE. However, if one detects certain AE modes, the doublet structure becomes apparent, and the staging of fault evolution manifests clearly (Fig. 6b). The AE mode I has only one specific *b-value* during shear, and variations are random. A more pronounced variation is observed if compared to the regular stick-slip. This probably results from the peculiarities of self-organization when fast and slow slip events take turns. The AE mode II shows staging of *b-value* alteration. The *b-value* decreases before each of the dynamic events and recover after them.

So, we can say that two AE subpopulations are emitted during gouge-filled fault sliding. These subpopulations have different scaling characteristics and different peculiarities of evolution. The obtained results indirectly indicate that two dynamic sub-systems emerge in the course of fault evolution at the meso-scale. One of the sub-systems exhibits scaling invariance in time, and structural changes are accompanied by AEs with harsh onsets (mode I). The other sub-system demonstrates periodical variations of scaling parameters in time, and the transition to the critical state is accompanied by an increase of the specific scale of structural alterations. The evolution of the second subsystem is accompanied by AEs with a gradual amplitude rise (mode II), which are less intensive.

4. Discussion

The obtained results improve our understanding of the processes at the micro-level. Both fast and slow slip events can be triggered at the micro-level. Some investigators reported emission of AEs with different waveforms in laboratory tests (Zigone et al., 2011; Ostapchuk et al., 2016; Hulbert et al., 2019), but no systematic analysis was performed. It should be noted that laboratory experiments are by no means a sort of scale modeling since it is simply impossible to fulfill all the similarity criteria in this case (Rosenau et al., 2017). Results of laboratory experiments should be considered as insights into fundamental properties of geomaterials and their structural peculiarities which determine fault slip behavior.

Most works consider the regime of regular stick-slip, when slip events take place quasi-periodically. However, there are only few natural faults, where characteristic earthquakes quasi periodically reoccur in time (Ben-Zion, 2008). So, we believe that the stochastic sliding regime with aperiodic slip events is more realistic. Improving methods of seismic signal processing point to ambiguity in slow slip event (SSE) scaling. In some areas SSE duration (T) and seismic magnitude (M_0) scale nearly linearly (Peng, Gomberg, 2010), while, for example, the Cascadia slow-slip events manifest a cubic moment-duration scaling and can produce pulse-like ruptures similar to fast slip events (Michel, et al., 2019). Shallow SSEs occur in the zone of highly overpressured fluids, low effective stress and transitional frictional behavior (Saffer, Wallace, 2015).

In the presented experiments the emission of AE waves is produced by the frictional instability. The spectrum of slip behaviors is governed by frictional dynamics via the interaction of the contact frictional properties, the effective normal stress and the elastic stiffness of the surrounding material (Leeman et al., 2016). The evolution of our model gouge-filled fault is controlled by peculiarities of formation and destruction of conglomerates of loaded grains at the meso-scale, the so called 'force chains' (Mair et al., 2002; Hayman et al., 2011; Lherminier et al., 2019). The assembly of these chains has a certain spatial structure and a relatively low specific weight inside the medium (Gao et al., 2019). Thus, two structural subsystems emerge inside a stressed fault – a consolidated force skeleton and rather moveable unconsolidated areas. We had no chance to visualize the inner processes of self-organization in the performed experiments, but we believe that the detected regularities of AE alteration do result from the evolution of the two structural subsystems. Probably, the change of force skeleton is accompanied by emission of the AE mode I, while the dynamics of unconsolidated areas – by AE mode II (Gao et al., 2019; Ostapchuk et al., 2020). We suggest that triggering AE mode II is, probably, supported by low effective normal stresses, analogous to the case of shallow SSEs. Certainly, the suggestions we have made require further specifications. Nevertheless, the emergence of AE doublet structure in all our experiments points to a fundamental properties of the effect.

Improving the methods to detect weak earthquakes and their statistical analysis allows to obtain an important information about fault dynamics and to trace the nucleation of an earthquake (Trugman, Ross, 2019; Gulia, Wiemer, 2019). In our experiments detecting the doublet structure of AE population can form a new basis for determining the critical state of slip event nucleation. A simple criterion of an "alarm" has been formulated. It is based on tracing specific acoustic manifestations of fault evolution in time - "If for the AE mode II for three successively estimated *b-values* a monotonic decrease is observed $b(t_{i-2}) > b(t_{i-1}) > b(t_i)$, then the alarm starts at the moment t_i. The end of the alarm is the moment when the slip event starts (the "true" alarm), or the moment t_n, when an increase of *b-value* is observed again $b(t_{n-1}) < b(t_n)$ (the "false" alarm) (Fig. 7, the inset). Fig. 7 presents variations of *b-value* in time for the AE mode II and "the raise of alarm" of the transition of the fault to the critical state.

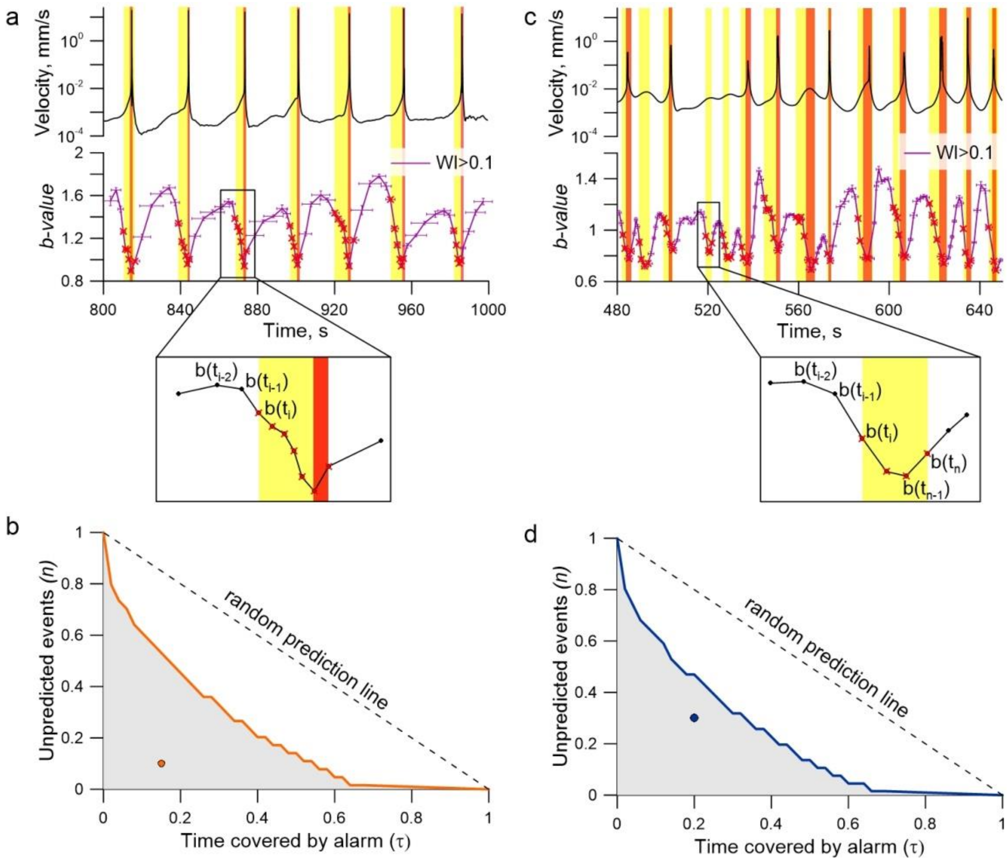

Figure 7. Transition of the model fault to the critical state.

Variations of block velocity and b-value of the AE mode II for a regular stick-slip in Exp.4 (a) and a stochastic sliding regime in Exp.13 (b). The yellow areas correspond to alarm intervals, the red ones – to slip events. Insets show mechanisms of a "true" alarm (a) and a "false" alarm (c).

We use Molchan's diagram to evaluate the predictive power for regular (c) and stochastic (d) sliding regimes. Shaded circles show the performance of prediction algorithm. Random binomial predictions occupy the diagonal. Random predictions with fixed alarm time (τ) fall in the grey area with the probability of $\alpha=10^{-5}$.

During a regular stick-slip (Fig. 7a) the duration of the alarm was 3.9±1.9s, while the recurrent time of dynamic failures was 34.2±0.8s. The alarm covers the whole pre-seismic stage of the seismic cycle. At the same time, it is important to note that the critical stage (when an event can be triggered by a weak disturbance) emerges at stresses close to the critical ones at the end of the pre-seismic stage (Kocharyan et al., 2018). For the stochastic regime (Fig. 7b) the pattern of *b-value* alteration is more complex, but the chosen alarm criterion is sensitive for such a regime too. A decrease of *b-value* signifies both the forthcoming fast and slow slip events, but more complex mechanisms of self-organization lead to "false alarms" (Ren et al., 2019) (Fig.7b, the inset).

The established criterion of the transition of a fault to the critical state should be considered as a step to understanding the basic earthquake nucleation mechanism and to improve the estimation of seismic hazard. The Molchan's error diagram is used to evaluate the predictive power of our prediction algorithm and its stability (Molchan, 2003; Molchan, 2010). We use two interdependent measures of prediction quality: the fraction of unpredicted events ν, and the fraction of alarms τ. Each prediction corresponds to a single point in (τ, ν) space. The error diagram for our prediction of the transition of the fault to the critical state of seismic cycle is presented in Fig. 7c,d. The τ-axis corresponds to the relative alarm time, the ν-axis – to the share of missed slip events. An extremely simple but easily tractable model of prediction which produces alarms independent of the target earthquakes is the random binomial prediction (Molchan, 2003; Shebalin et al., 2006). The probability for a random binomial prediction with a given value of τ to fall within the shaded area is less than or equal to 10^{-5} (0.001 %). The point corresponds to our prediction algorithm indicating very high predictive power both for the regular and the stochastic sliding regimes. The efficiency of the precursor J_m is defined as:

$$J_m = 1 - \nu - \tau, \tag{8}$$

The value of J_m lies in the range of (0…1). The nearer the value to 1 is, the more reliable is the raise of alarm. In our experiments the efficiency of the method for a regular stick-slip is J_m = 0.59…0.83, while for the stochastic sliding regime that includes both fast and slow slip modes the value is J_m = 0.4…0.65 (Supplementary Table S1). For comparison, the efficiency of the ETAS forecasting model for earthquakes M>6 in Southern California is 0.29 (Lippiello et al., 2012). Predictions based on the ultralow frequency magnetic data show the efficiency of about 0.23 (Han et al., 2017). The forecasting technique based on the effect of modulation of high frequency seismic noise in Kamchatka gives the value of about 0.5 for target earthquakes M≥6 (Saltykov, 2017). Thus, the prediction criterion based on detecting the doublet structure of the ensemble of AEs turns to be highly effective both for fast and for slow slip events. This testifies that a spectrum of frictional fault slip modes share a common mechanism.

5. Conclusions

A unified pattern of fault slip behavior evolution is a fundamental issue. It requires linking seismic, mechanical and structural data. In the present study, we have revealed the doublet structure of AE population, which reflects the complexity of internal fault structure at the meso-scale. Both fast and slow events are initiated at the micro-scale. Different scaling relations are intrinsic to those events. At the same time at the macro-scale we observed a similar pattern of nucleation of both fast and slow slip events. This allows us to speak about the unity of physical mechanisms of nucleation of entire spectrum of fault slip modes. Revealing the doublet structure of AE population and tracing scaling parameters of AE subpopulations allows us to introduce a new short-term precursor, that may improve the seismic hazard assessment.

Acknowledgements

This work was partially supported by RFBR and NSFC according to the research project No. 20-55-53031 for K.G.M., D.V.P. & A.A.O. V.K.M & M.F.P. acknowledge Program No. AAAA-A17-117 112350020-9 of The Ministry of Science and Higher Education of the Russian Federation.

Data availability. All the data that support findings of this work were collected on geomechanical test bench of the Sadovsky Institute for Dynamics of Geospheres of Russian Academy of Sciences. All data set used in this paper are available on Mendeley Data (doi: 10.17632/kykwmjmpgf.1)

References

Anthony, J.L., Marone, C., 2005. Influence of particle characteristics on granular friction. J. Geophys. Res. 110, B08409. https://doi.org/10.1029/2004JB003399.

Ben-Zion, Y., 2008. Collective behavior of earthquakes and faults: Continuum–discrete transitions, progressive evolutionary changes, and different dynamic regimes. Reviews of Geophysics 46, 1–70. doi: 10.1029/2008RG000260.

Besedina, A.N., Kishkina S.B., Kocharyan, G.G., et al. 2020. Weak induced seismicity in the Korobkov iron ore field of the Kursk magnetic anomaly. Journal of Mining Science 56 (3), (in press).

Burgmann, R., 2018. The geophysics, geology and mechanics of slow fault slip // Earth and Planetary Science Letters 495, 112–134. https://doi.org/10.1016/j.epsl.2018.04.062.

Cicerone, R.D., Ebel, J.E. & Britton, J.A., 2009. A systematic compilation of earthquake precursors. Tectonophysics 476, 371-396. https://doi.org/10.1016/j.tecto.2009.06.008

Cruz-Atienza, V.M., Villafuerte, C., Bhat, H.S., 2018. Rapid tremor migration and pore-pressure waves in subduction zones. Nat.Commun 9, 2900. https://doi.org/10.1038/s41467-018-05150-3.

de Arcangelis, L., Cataldo Godano, C., Grasso, J.R., Lippiello, E., 2016. Statistical physics approach to earthquake occurrence and forecasting. Physics Reports, 628, 1-91. https://doi.org/10.1016/j.physrep.2016.03.002.

Frank, W., Shapiro, N.M., Husker, A., Kostoglodov, V., Gusev, A.A., & Campillo, M., 2016. The evolving interaction of lowfrequency earthquakes during transient slip. Science Advances, 2(4), e1501616. https://doi.org/10.1126/sciadv.1501616.

Gao, K., et al., 2019. From stress chains to acoustic emission. Phys. Rev. Lett. 123, 048003, doi: 10.1103/PhysRevLett.123.048003.

Gerasimova, T.I., Kondratev, V.N. & Kocharyan, G.G., 1995. Modeling features of shear deformation of fissures containing filler. Journal of Mining Science 31 (4), 288-295, doi: 10.1007/BF02048229.

Gulia, L., Wiemer, S. 2019. Real-time discrimination of earthquake foreshocks and aftershocks. Nature 574, 193–199. https://doi.org/10.1038/s41586-019-1606-4

Hayman, N.W., et al., 2011. Granular controls on periodicity of stick-slip events: kinematics and force-chains in an experimental fault. Pure Appl. Geophys. **168**, 2239. doi: 10.1007/s00024-011-0269-3.

Hulbert, C., Rouet-Leduc, B., Johnson, P.A. et al. 2019. Similarity of fast and slow earthquakes illuminated by machine learning. Nature Geosci 12, 69–74. https://doi.org/10.1038/s41561-018-0272-8.

Johnson, P.A., Ferdowsi, B., Kaproth, B.M. et al. 2013. Acoustic emission and microslip precursors to stick-slip failure in sheared granular material. Geophysical Research Letters 40, 1-5, doi: 10.1002/2013GL057848.

Johnson, P., Jia, X. 2005. Nonlinear dynamics, granular media and dynamic earthquake triggering. Nature 437, 871–874. https://doi.org/10.1038/nature04015

Kocharyan, G.G., 2016. Geomechanics of Faults. Moscow: GEOS. (in Russian)

Kocharyan, G.G., Novikov, V.A., Ostapchuk, A.A. & Pavlov, D.V., 2017. A study of different fault slip modes governed by the gouge material composition in laboratory experiments. Geophysical Journal International 208 (1), 521-528, doi: 10.1093/gji/ggw409.

Kocharyan, G.G., Markov, V.K., Ostapchuk, A.A. et al., 2014. Mesomechanics of shear resistance along a filled crack. Phys Mesomech 17, 123–133. https://doi.org/10.1134/S1029959914020040

Kocharyan, G.G., Ostapchuk, A.A. 2011. Variations in rupture zone stiffness during a seismic cycle. Dokl. Earth Sc. 441, 1591, https:// doi.org/10.1134/S1028334X11110250.

Kocharyan, G.G., Ostapchuk, A.A., Pavlov, D.V., 2018. Traces of laboratory earthquake nucleation in the spectrum of ambient noise. Sci. Rep. 8, 10764, https://doi.org/10.1038/s41598-018-28976-9.

Kocharyan, G.G., Ostapchuk, A.A., Pavlov, D.V., Markov, V.K., 2018. The effects of weak dynamic pulses on the slip dynamics of a laboratory fault. Bulletin of the Seismological Society of America, 108(5B), 2983–2992. https://doi.org/10.1785/0120170363.

Leeman, J., Saffer, D., Scuderi, M., et al., 2016. Laboratory observations of slow earthquakes and the spectrum of tectonic fault slip modes. Nat Commun 7, 11104, doi:10.1038/ncomms11104.

Lei, X., Li, S., Liu, L., 2018. Seismic b-value for foreshock AE events preceding repeated stick-slips of pre-cut faults in granite. Appl. Sci. 8, 2361. https://doi.org/10.3390/app8122361.

Lei, X. 2003. How does asperities fracture? An experimental study of unbroken asperities. Earth and Planetary Science Letters 213, 347-359, doi; 10.1016/S0012-821X(03)00328-5.

Lherminier, S., Planet, R., Levy dit Vehel, V. et al., 2019. Continuously Sheared Granular Matter Reproduces in Detail Seismicity Laws. Phys. Rev. Lett. 122, 218501, doi: 10.1103/PhysRevLett.122.218501.

Lippiello, E., Marzocchi, W., de Arcangelis, L. et al., 2012. Spatial organization of foreshocks as a tool to forecast large earthquakes. Sci Rep 2, 846, https://doi.org/10.1038/srep00846.

Mair, K., Frye, K.M., Marone, C., 2002. Influence of grain characteristics on the friction of granular shear zones. J. Geophys. Res. 107, 10, 2219. https://doi.org/10.1029/2001JB000516

Marone, C., 1998. Laboratory-derived friction laws and their application to seismic faulting. Annu. Rev. Earth. Planet. Sci. 26, 643-696. https://doi.org/10.1146/annurev.earth.26.1.643

Michel, S., Gualandi, A., Avouac, J.-P., 2019. Similarity scaling laws for earthquakes and Cascadia slow-slip events. Nature. 574, 522-526, DOI: 10.1038/s41586-019-1673-6.

Molchan, G.M., 2003. Earthquake Prediction Strategies: A Theoretical Analysis. In: Keilis-Borok V.I., Soloviev A.A. (eds) Nonlinear Dynamics of the Lithosphere and Earthquake Prediction. Springer Series in Synergetics. Springer, Berlin, Heidelberg https://doi.org/10.1007/978-3-662-05298-3_5

Molchan., G., 2010. Space–Time Earthquake Prediction: The Error Diagrams. Pure Appl. Geophys. 167, 907–917, DOI 10.1007/s00024-010-0087-z.

Nielsen, S., 2017. From slow to fast faulting: recent challenges in earthquake fault mechanics. Phil. Trans. R. Soc. A 375, 20160016. http://dx.doi.org/10.1098/rsta.2016.0016

Nishitsuji, Y., Mori, J., 2014. Source parameters and radiation efficiency for intermediate-depth earthquakes in Northeast Japan, Geophysical Journal International 196, 2, 1247–1259, https://doi.org/10.1093/gji/ggt458.

Ostapchuk, A.A., Morozova, K.G., 2020. On the mechanism of laboratory earthquake nucleation highlighted by acoustic emission. Sci.Rep 10, 7245. https://doi.org/10.1038/s41598-020-64272-1.

Ostapchuk, A.A., Morozova, K.G. & Pavlov, D.V., 2019b. Influence of the structure of a gouge-filled fault on the parameters of acoustic emission. Acta Acustica united with Acustica 105, 759–765, https://doi.org/10.3813/AAA.919356.

Ostapchuk, A.A., Pavlov, D.V., Markov, V.K., Krasheninnikov, A.V. 2016. Study of acoustic emission signals during fracture shear deformation. Acoust. Phys. 62, 505-513, doi: 10.1134/S1063771016040138.

Ostapchuk, A.A., et al. 2019a. Seismic-acoustics of a block sliding along a fault. Pure Appl. Geophys. https://doi.org/10.1007/s00024-019-02375-1.

Peng, Z., Gomberg, G., 2010. An integrated perspective of the continuum between earthquakes and slow-slip phenomena. Nat. Geosci. 3,599–607. doi: 10.1038/ngeo940.

Peng, H., Hattori, K., Zhuang, J., et al., 2017. Evaluation of ULF seismo-magnetic phenomena in Kakioka, Japan by using Molchan's error diagram. Geophysical Journal International 208, 1, 482–490. https://doi.org/10.1093/gji/ggw404.

Reber, J., Lavier, L., & Hayman, N., 2015. Experimental demonstration of a semi-brittle origin for crustal strain transients. Nature Geosci 8, 712–715. https://doi.org/10.1038/ngeo2496.

Ren, C.X., Dorostkar, O., Rouet-Leduc, B., et al., 2019. Machine learning reveals the state of intermittent frictional dynamics in a sheared granular fault. Geophysical Research Letters 46, 7395-7403, doi: 10.1029/2019GL082706.

Riviere, J., Lv Z., Johnson, P. & Marone, C. 2018. Evolution of b-value during the seismic cycle: Insights from laboratory experiments on simulated faults. Earth Planet. Sci. Lett. 482, 407-413, doi: 10.1016/j.epsl.2017.11.036.

Rosenau, M., Corbi, F. & Dominguez, S., 2017. Analogue earthquakes and seismic cycles: experimental modeling across timescales. Solid Earth 8, 597-635, doi: 10.5194/se-8-597-2017.

Rundle, J.B., Holliday, J.R., Yoder, M., 2011. Earthquake precursors: activation or quiescence? Geophys. J. Int. 187, 225-236, doi: 10.1111/j.1365-246X.2011.05134.x.

Saltykov, V.A., 2017. On the possibility of using the tidal modulation of seismic waves for forecasting earthquakes. Izv., Phys. Solid Earth 53, 250–261. https://doi.org/10.1134/S1069351317010128.

Scuderi, M. et al. 2016. Precursory changes in seismic velocity for the spectrum of earthquake failure modes. Nature Geosci. 9, 695–700, https://doi.org/10.1038/ngeo2775.

Scholz, C.H., 2002. The mechanics of earthquakes and faulting. Cambridge: Cambridge University Press.

Scuderi, M.M., Collettini, C., Vinti, C., Marone, C., 2017. Evolution of shear fabric in granular fault gouge from stable sliding to stick slip and implications for fault slip mode. Geology 45 (8), 731-734, doi: 10.1130/G39033.1.

Shebalin, P., Keilis-Borok, V., Gabrielov, A., Zaliapin, I., Turcotte, D., 2006. Short-term earthquake prediction by reverse analysis of lithosphere dynamics. Tectonophysics 413, 1-2, 63-75. https://doi.org/10.1016/j.tecto.2005.10.033.

Shiotani, T., Ohtsu, M., Ikeda, K., 2001. Detection and evaluation of AE waves due to rock deformation. Construction and Building Materials 15, 5–6, 235-246. https://doi.org/10.1016/S0950-0618(00)00073-8.

Trugman, D.T., Ross, Z.E., 2019. Pervasive foreshock activity across Southern Califirnia. Geophys. Res. Lett. 46, 8772-8781. https://doi.org/10.1029/2019GL083725.

Turcotte, D.L., 1999. Self-organized criticality. Rep. Prog. Phys. 62 1377 https://doi.org/10.1088/0034-4885/62/10/201.

Veedu, D.M., Barbor, S. 2016. The Parkfield tremors reveal slow and fast ruptures on the same asperity. Nature 532, 361–365. doi: 10.1038/nature17190.

Villegas-Lanza, J., Nocquet, J., Rolandone, F. et al., 2016. A mixed seismic–aseismic stress release episode in the Andean subduction zone. Nature Geosci 9, 150–154. https://doi.org/10.1038/ngeo2620.

Saffer, D., Wallace, L. 2015. The frictional, hydrologic, metamorphic and thermal habitat of shallow slow earthquakes. Nature Geosci 8, 594–600. https://doi.org/10.1038/ngeo2490

Zigone, D., Voisin, C., Larose, E., Renard, F., Campillo, M. 2011. Slip acceleration generates seismic tremor like signals in friction experiments. Geophys. Res. Lett. 38, L01315. https://doi.org/10.1029/2010GL045603

Zhuo, Y.-Q., Liu, P., Chen, S., et al., 2018. Laboratory observations of tremor-like events generated during preslip. Geophysical Research Letters 45 (14), doi: 10.1029/2018GL079201.

References from Supporting Information

Burgmann, R., 2018. The geophysics, geology and mechanics of slow fault slip. Earth and Planetary Science Letters 495, 112–134. https://doi.org/10.1016/j.epsl.2018.04.062.

Hanks, T., Kanamori, H., 1979. A moment magnitude scale. J. Geophys. Res. 84, 2348–2350. https://doi.org/10.1029/JB084iB05p02348.

Lei, X., 2003. How does asperities fracture? An experimental study of unbroken asperities. Earth and Planetary Science Letters 213, 347-359. https://doi.org/10.1016/S0012-821X(03)00328-5.

Figure 1.

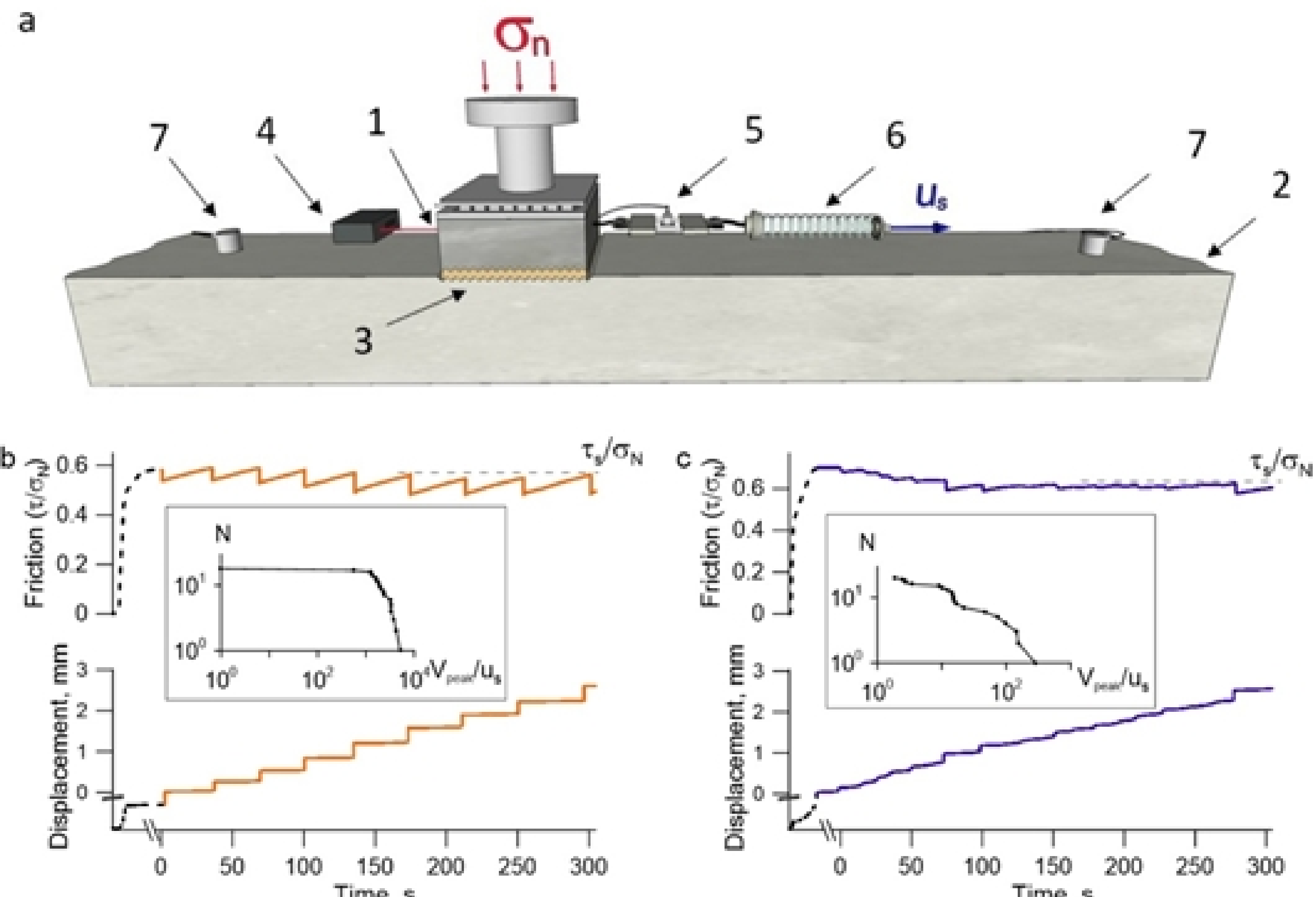

a
σ_n
1
2
3
4
5
6
7
7
u_s
b
c
τ_s/σ_N
Friction (τ/σ_N)
Displacement, mm
Time, s
N
V_{peak}/u_s

Figure 2.

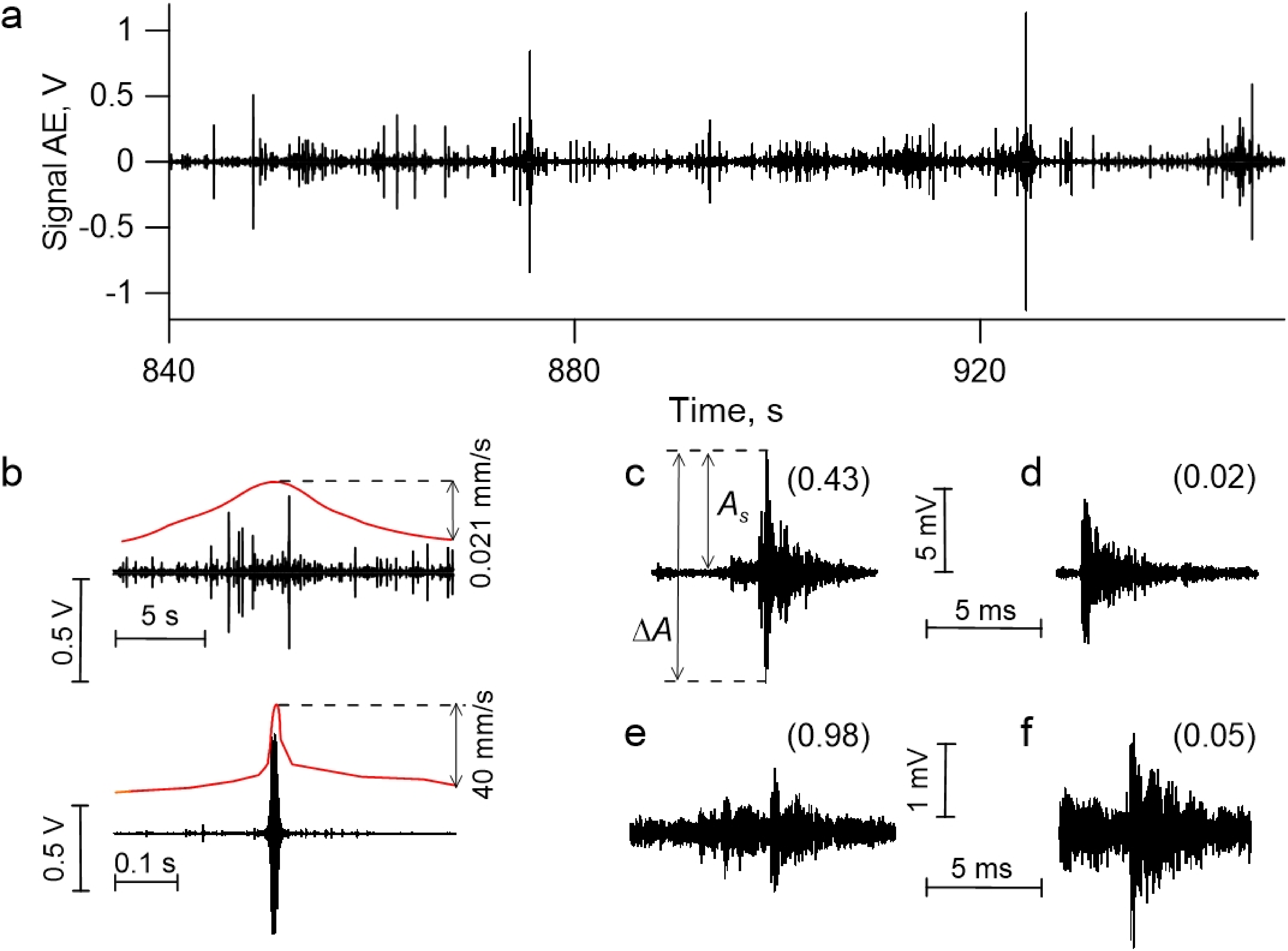

a
Signal AE, V
1
0.5
0
-0.5
-1
840
880
920
Time, s
b
0.021 mm/s
0.5 V
5 s
40 mm/s
0.5 V
0.1 s
c
(0.43)
A_s
ΔA
d
(0.02)
5 mV
5 ms
e
(0.98)
f
(0.05)
1 mV
5 ms

Figure 3.

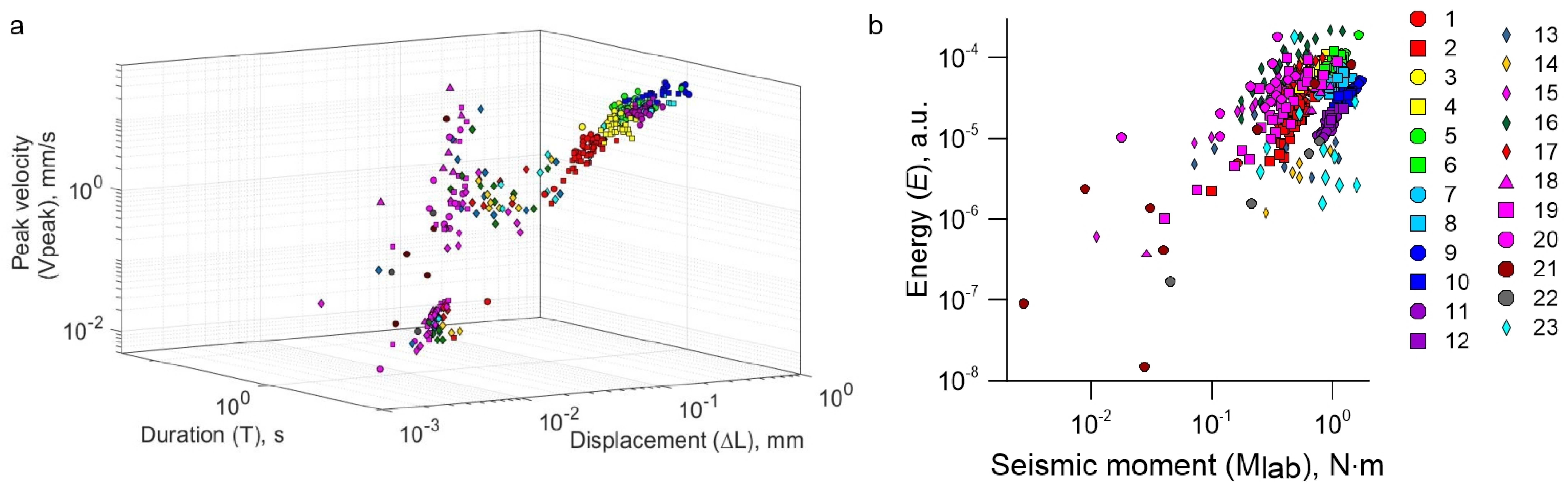

a
Peak velocity (Vpeak), mm/s
Duration (T), s
Displacement (ΔL), mm
b
Energy (E), a.u.
Seismic moment (Mlab), N·m
1
2
3
4
5
6
7
8
9
10
11
12
13
14
15
16
17
18
19
20
21
22
23

Figure 4.

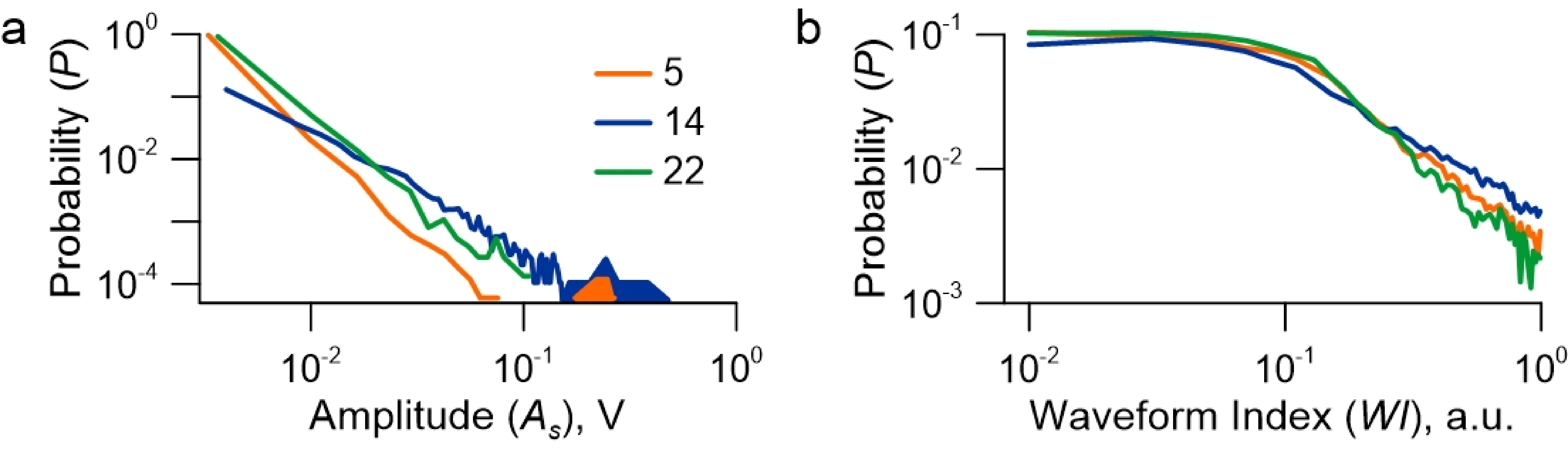
a
Probability (P)
10^0
10^-2
10^-4
5
14
22
10^-2
10^-1
10^0
Amplitude (A_s), V
b
Probability (P)
10^-1
10^-2
10^-3
10^-2
10^-1
10^0
Waveform Index (WI), a.u.

Figure 5.

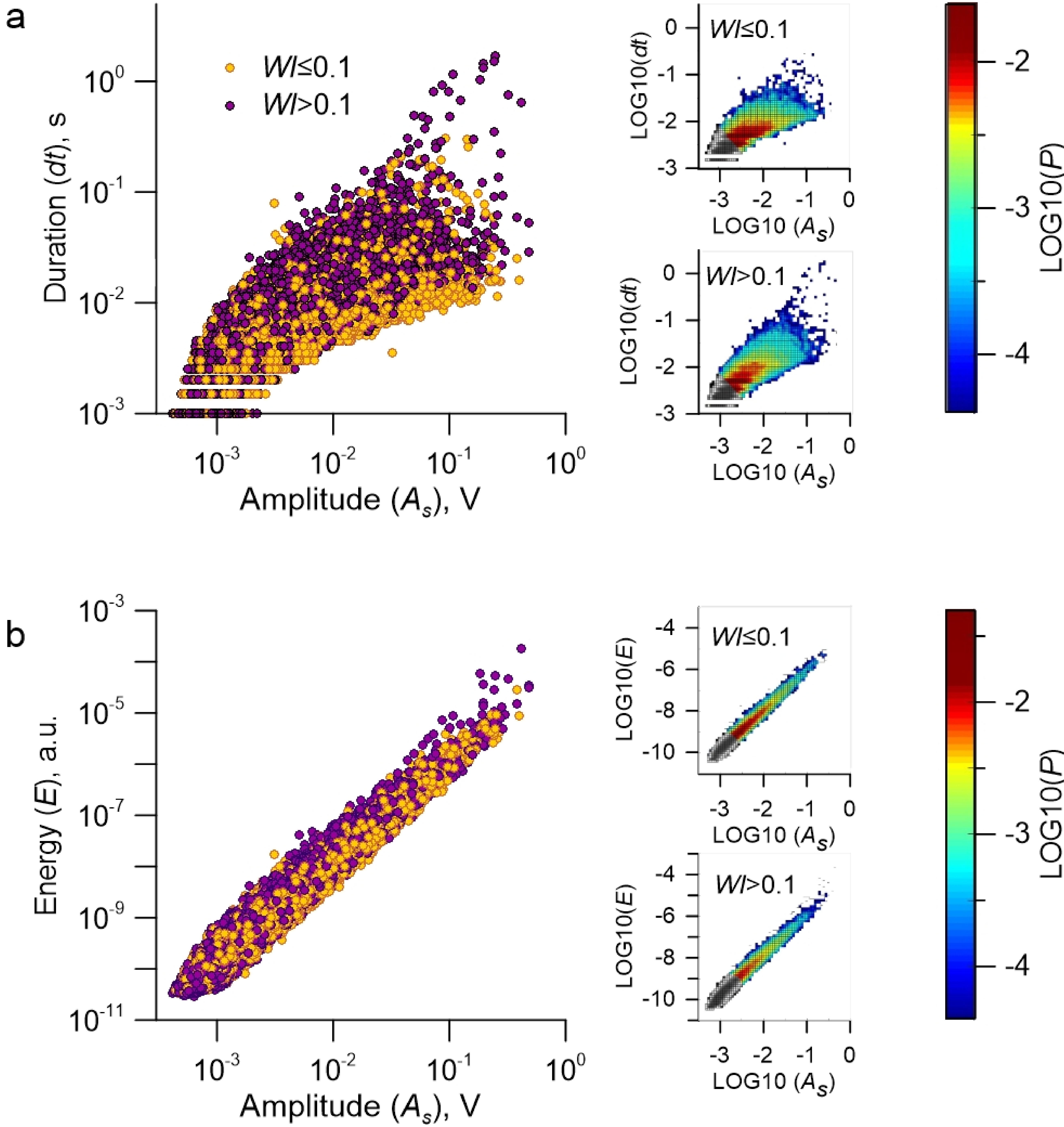

a
WI≤0.1
WI>0.1
Duration (dt), s
Amplitude (As), V
LOG10(dt)
LOG10 (As)
LOG10(P)
b
Energy (E), a.u.
Amplitude (As), V
LOG10(E)
LOG10 (As)
LOG10(P)

Figure 6.

a
b
Velocity, mm/s
10^0
10^{-2}
10^{-4}
Amplitude (A_s), V
AE rate, s^{-1}
160
80
0
120
60
10^{-1}
10^{-3}
Time, s
880
920
960
1000
560
600
640
680
b-value
1.6
1.2
0.8
0.4
WI≤0.1
WI>0.1
0.1
Probability (P)

Figure 7.

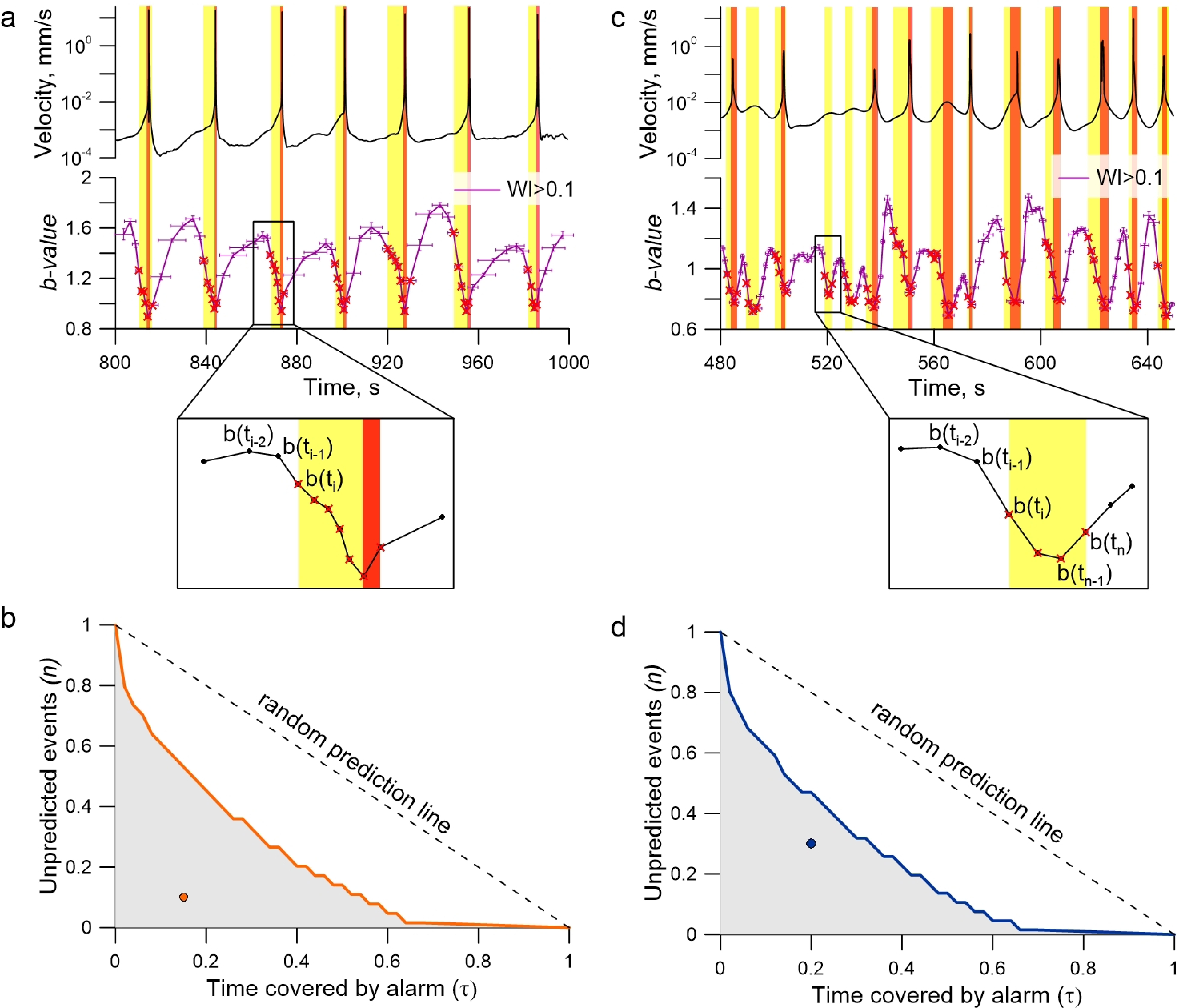

a
Velocity, mm/s
b-value
WI>0.1
Time, s
b(t_{i-2})
b(t_{i-1})
b(t_i)
c
b(t_n)
b(t_{n-1})
b
Unpredicted events (n)
Time covered by alarm (τ)
random prediction line
d